






REVIEW

Structural basis of cytoplasmic Na_v1.5 and Na_v1.4 regulation

Sara Nathan¹ , Sandra B. Gabelli^{1,2,3} , Jesse B. Yoder¹, Lakshmi Srinivasan¹ , Richard W. Aldrich⁴ , Gordon F. Tomaselli⁵, Manu Ben-Johny⁶ , and L. Mario Amzel^{1,3}

Voltage-gated sodium channels (Na_vs) are membrane proteins responsible for the rapid upstroke of the action potential in excitable cells. There are nine human voltage-sensitive Na_v1 isoforms that, in addition to their sequence differences, differ in tissue distribution and specific function. This review focuses on isoforms Na_v1.4 and Na_v1.5, which are primarily expressed in skeletal and cardiac muscle cells, respectively. The determination of the structures of several eukaryotic Na_vs by single-particle cryo-electron microscopy (cryo-EM) has brought new perspective to the study of the channels. Alignment of the cryo-EM structure of the transmembrane channel pore with x-ray crystallographic structures of the cytoplasmic domains illustrates the complementary nature of the techniques and highlights the intricate cellular mechanisms that modulate these channels. Here, we review structural insights into the cytoplasmic C-terminal regulation of Na_v1.4 and Na_v1.5 with special attention to Ca²⁺ sensing by calmodulin, implications for disease, and putative channel dimerization.

Introduction

Voltage-gated sodium channel architecture in excitable cells

Voltage-gated sodium channels (Na_vs) are integral membrane ion channels that open upon depolarization to allow an influx of Na⁺ ions down their concentration gradient. This Na⁺ current (I_{Na}) further depolarizes the cell, resulting in the opening of other voltage-gated ion channels and generating an action potential. This role makes Na_v channels key participants in the initiation of action potentials and in the excitation–contraction of muscle cells. Of the nine Na_v1 isoforms, skeletal muscle cells express Na_v1.4 and cardiac muscle cells (cardiomyocytes) express Na_v1.5, the two isoforms that are the focus of this review. (Yu and Catterall, 2003; Jo et al., 2004; Yu et al., 2005). In addition to its well-recognized role in the heart, Na_v1.5 has been shown to contribute to gastrointestinal motility through expression in the pacemaker interstitial cells of Cajal and circular smooth muscle cells in the jejunal small intestine (Holm et al., 2002; Ou et al., 2002; Strege et al., 2003). Like those in the cardiac muscle, these cells are electrochemically coupled by gap junctions to facilitate rapid, rhythmic excitation and contraction of the tissue.

Na_v channels consist of a pore-forming α-subunit and one or more auxiliary β-subunits that regulate voltage dependence,

gating kinetics, and channel density. β-Subunits fold as an extracellular IgG domain with a single transmembrane domain. The α-subunits (Fig. 1) are pseudotetramers that are roughly 2,000 amino acids in length with 4 transmembrane domains (DI–DIV), each of which contains 6 membrane-spanning α-helices (S1–S6). Together, the four domains form the pore of the channel that opens to allow an inward Na⁺ current (Marban et al., 1998). S1–S4 of each of these domains form the voltage-sensing domain (VSD) that shifts to open the pore formed by S5 and S6 (Fig. 1b). An α-helix between S5 and S6 re-embeds into the extracellular side of the membrane to form the narrow ion-selective filter (McCusker et al., 2012; Lenaeus et al., 2017; Wisedchaisri et al., 2019). The linker between DIII and DIV forms the fast inactivation gate containing a hydrophobic Ile-Phe-Met (IFM) motif that blocks the intracellular mouth of the pore to stem the Na⁺ current following the channel's activation. The C terminus (CTNa_v; ~200–300 amino acids in length) projects into the cytoplasm of the cell where it binds several channel-interacting proteins, including the cellular calcium sensor calmodulin (CaM) and fibroblast growth homologous factors (FHF; Liu et al., 2001, 2003; Goetz et al., 2009). These

¹Department of Biophysics and Biophysical Chemistry, Johns Hopkins University School of Medicine, Baltimore, MD; ²Division of Cardiology, Department of Medicine, Johns Hopkins University School of Medicine, Baltimore, MD; ³Department of Oncology, Johns Hopkins University School of Medicine, Baltimore, MD; ⁴Department of Neuroscience, University of Texas at Austin, Austin, TX; ⁵Division of Cardiology, Department of Medicine, Albert Einstein College of Medicine, Bronx, NY; ⁶Department of Physiology and Cellular Biophysics, Columbia University, New York, NY.

Correspondence to Sandra B. Gabelli: gabelli@jhmi.edu; L. Mario Amzel: mamzel@jhmi.edu; J.B. Yoder's present addresses are Hauptman-Woodward Medical Research Institute, Buffalo, NY; and Industrial Macromolecular Crystallography Association—Collaborative Access Team, Advanced Photon Source, Argonne National Laboratory, Argonne, IL.

© 2020 Nathan et al. This article is distributed under the terms of an Attribution–Noncommercial–Share Alike–No Mirror Sites license for the first six months after the publication date (see <http://www.rupress.org/terms/>). After six months it is available under a Creative Commons License (Attribution–Noncommercial–Share Alike 4.0 International license, as described at <https://creativecommons.org/licenses/by-nc-sa/4.0/>).

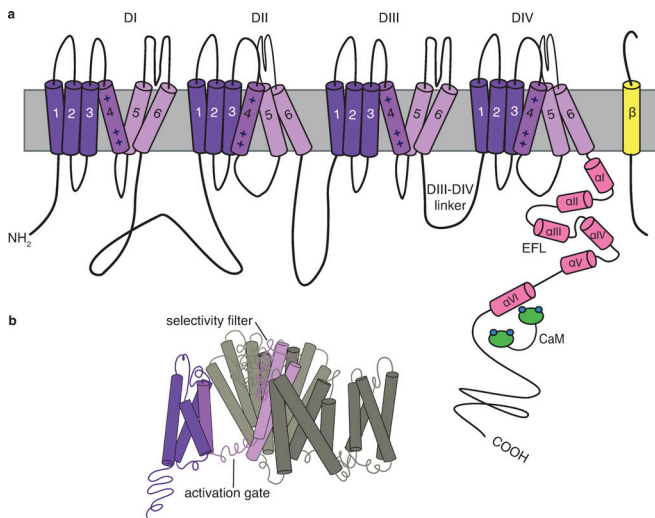


Figure 1. Schematic of NaVs. (a) The NaVs are pseudotetramers with four transmembrane domains (DI–DIV, purple), with each domain containing six α -helices (S1–S6). The cytoplasmic CT has been shown to have six α -helices (α I– α VI; pink) with α I– α VI forming the EFL. (b) The open configuration of the transmembrane domains, with S1–S6 of one domain shaded in purple to show S1–S4 (dark purple) forming the VSD that shifts to open the pore formed by S5–S6 (light purple).

FHFs have been understood to diverge from secreted fibroblast growth factors in being restricted to the cytoplasm, but it has recently been shown that they do activate extracellular fibroblast growth factor receptors (Sochacka et al., 2020). Na_v1.4 and Na_v1.5 are also regulated by and have C terminus (CT) binding sites for the E3 ligase NEDD4L and various syntrophins, though structural information has yet to be published for these regions (Fotia et al., 2004; Gavillet et al., 2006; Petitprez et al., 2011).

Advances in the resolution of single-particle cryo-EM have had a significant impact on the elucidation of the structures of large transmembrane proteins. Na_v channel structures from several species, under different conditions and with various partners, have provided a structural basis for the design of new experiments. Importantly, eukaryotic Na_v channels are large, single-chain pseudotetramers in contrast to prokaryotic channels—used in the pioneering structure determinations—which are true homotetramers composed of four assembled transmembrane subunits. This distinction is significant for understanding channel biology and makes these cryo-EM structure determinations invaluable additions to the field. The Na_v channels perfectly illustrate the complementarity between cryo-EM and x-ray crystallography: cryo-EM studies report the structures of the large channel pores, but almost without exception fail to resolve the cytoplasmic portions of the channel, whereas x-ray crystallographic structures provide high-resolution snapshots of these regions. In particular, CTNa_v and its interacting partners have been expressed as soluble proteins and the subject of extensive x-ray diffraction and thermodynamic studies. The cryo-EM structure of the cockroach Na_v (Protein Data Bank [PDB] accession no. 5X0M) contained sufficient coverage of intracellular channel regions along with the transmembrane pore to allow

alignment with the cytoplasmic CTNa_v and provide an increasingly complete view of the channel. This review uses a structural perspective to provide a rationale for how cytoplasmic channel interactions relate to its biology.

CaM regulation of excitation–contraction

CaM is a ubiquitously expressed 148-amino acid protein that folds into two globular lobes (N- and C-lobe) connected by a flexible linker. The N- and C-lobes each contain two EF hands that can bind one Ca²⁺ each. EF hands themselves are formed by two α -helical sequences oriented perpendicular to each other and connected by a Ca²⁺-binding loop. The C-lobe can be found in an open, semi-open, or closed conformation depending on Ca²⁺ occupancy, while the N-lobe has only been found to be open or closed in nature (Kawasaki and Kretsinger, 2012). Changes between these CaM configuration states upon binding Ca²⁺ subsequently alters binding to its many targets, earning the molecule's moniker, the cellular Ca²⁺ sensor.

CaM often targets basic amphipathic α -helical motifs, a category which encompasses the IQ motif (consensus sequence (I/L/V)QXXXRXXXX(R/K)) found in CTNa_v. IQ motifs may bind CaM even in its Ca²⁺-free configuration (apo-CaM; Bähler and Rhoads, 2002; Núñez et al., 2020). CaM has been shown to regulate many proteins that are critical to the excitation–contraction mechanism of muscle cells, including directly binding to channels such as voltage-gated Ca²⁺ channels, voltage-gated K⁺ channels, small conductance Ca²⁺-activated K⁺ channels, cyclic nucleotide-gated channels, RYR, and transient receptor potential channels as well as Na_v channels (Saimi and Kung, 2002; Kovalevskaya et al., 2013; Adelman, 2016).

Structural alignment of cytoplasmic CT with channel pore

In the last decade, a number of structures of CTNa_vs in complex with CaM have been determined by using x-ray crystallography or NMR (Table 1). The available structures of the CT (Fig. 2) reveal that, after domain DIV, all the published Na_v proteins fold as a five-helix EF hand-like (EFL) region followed by a long helix α VI containing the IQ motif that binds CaM. Early investigations hypothesized that this EF-analogous region gave the channels their Ca²⁺-sensitive properties, but it was later determined that the region did not bind Ca²⁺ and that CaM was mediating Ca²⁺ sensing (Peterson et al., 1999). In all structures of the CTNa_v–CaM complexes, the CaM C-lobe binds the IQ motif of helix α VI. Across the Na_v isoforms, the 50–70 amino acids following the IQ motif bear no significant sequence homology and no structural information is available for any of them.

Recently, the structures of several of the transmembrane portions of Na_v channels have been determined by using single-particle cryo-EM: for example, human Na_v1.7 (PDB accession no. 6J8J), human Na_v1.4 (PDB accession no. 6AGF), human Na_v1.2 (PDB accession no. 6J8E), rat Na_v1.5 (PDB accession nos. 6UZ3 and 6UZ0), and Na_vPas (*Periplaneta americana*; cockroach; PDB accession nos. 5X0M and 6A90) are shown in Fig. 3 (Shen et al., 2017; Pan et al., 2018; Pan et al., 2019; Shen et al., 2019; Wisedchaisri et al., 2019). These cryo-EM structures display the six transmembrane helices of each of the four domains, as well as some of the connecting intracellular and extracellular loops.

Table 1. **Published structures of CTNa_v with CaM**

PDB accession no.	Resolution	Na _v	Na _v residues	CaM	CaM/Ion	FHF	Year	Reference
2L53	NMR	1.5	1901–1927	WT	—	No	2011	Chagot and Chazin, 2011
2KXW	NMR	1.2	1901–1927	C-lobe	—	No	2011	Feldkamp et al., 2011
4DCK	2.20 Å	1.5	1773–1940	WT	—	FHF-2	2012	Wang et al., 2012
3WFN	1.95 Å	1.6	1893–1914	WT	—	No	2013	Reddy Chichili et al., 2013
4JPZ	3.00 Å	1.2	1784–1933	WT	Ca ²⁺	FHF-2	2014	Wang et al., 2014
4JQ0	3.84 Å	1.5	1773–1940	WT	Ca ²⁺	FHF-1	2014	Wang et al., 2014
4OVN	2.80 Å	1.5	1773–1929	WT	Mg ²⁺	No	2014	Gabelli et al., 2014
2M5E	NMR	1.2	1901–1927	C-lobe	Ca ²⁺	No	2014	Hovey et al., 2017
6BUT	NMR	1.2	1901–1927	WT	—	No	2019	—
6MBA	1.80 Å	1.4	1599–1764	WT	—	No	2018	Yoder et al., 2019
6MC9	3.30 Å	1.4	1599–1754	WT	Ca ²⁺	No	2018	Yoder et al., 2019
6MUD	2.69 Å	1.5	1785–1920	WT	Ca ²⁺	No	2019	Gardill et al., 2018
6MUE	1.90 Å	1.4	1721–1735	WT	Ca ²⁺	No	2019	Gardill et al., 2018

Pairwise alignment among the five structures shows an RMSD of ~2.5 Å for >900 C α s (relative to 5XOM). The CT was not resolved in these structures, with the exception of ~50 amino acids of the CT EFL of Na_vPas 5XOM (Fig. 4 a). Structural alignment of this portion of the Na_vPas with the EFL of the x-ray structure of, for example, the Na_v1.5 (PDB accession no. 4OVN), extends the coordinates of the model to include the regions of the channels that interact with CaM (Fig. 4 c; 0.39 RMSD over 69 amino acids).

Alignment of the EFL of the Na_vPas cryo-EM structure with that of the x-ray CTNa_v positions the second helix of the DIII–DIV linker between helices α I and α IV of the EFL. Notably, in the x-ray structure, the EFL binding site has been observed to be occupied by the α VI helix of another CTNa_v (Gabelli et al., 2014). The interaction of helix α VI with the EFL was also hypothesized by Chazin and observed by Glaaser (Chagot et al., 2009; Glaaser et al., 2012). Binding to the EFL by the DIII–DIV linker and by the

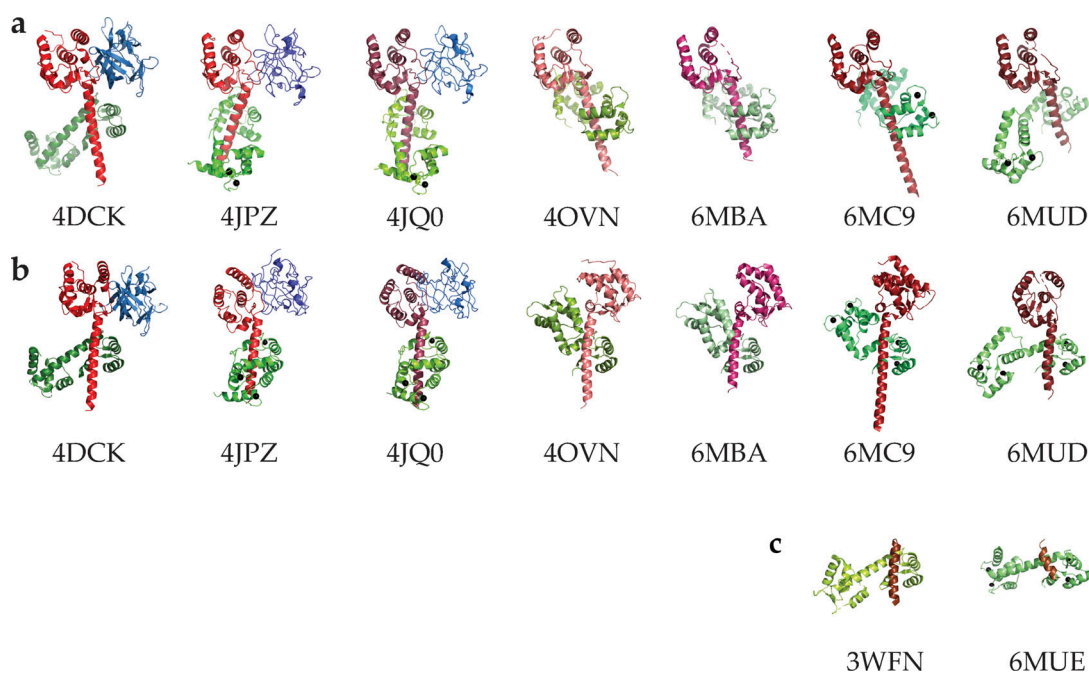


Figure 2. **Published crystal structures of CTNa_v with CaM.** (a) Structures aligned pairwise to CTNa_v1.5–CaM (PDB accession no. 4OVN) using the EFL domain as an anchor. Each CT is in shades of red, CaM in green, and FHF in blue. The angle of helix α VI with respect to the EFL varies in these constructs. (b) The same structures aligned pairwise using the CaM C-lobe as an anchor and so helix α VI has the same orientation. These alignments highlight the different relative orientations of the EFL and helix α VI, displaying the EFL to the right (4OVN, 6MBA, 6MC9) or to the left (4DCK, 4JPZ, 4JQ0, 6MUD). (c) Complexes of CaM with shorter peptides of CTNa_v1.5.

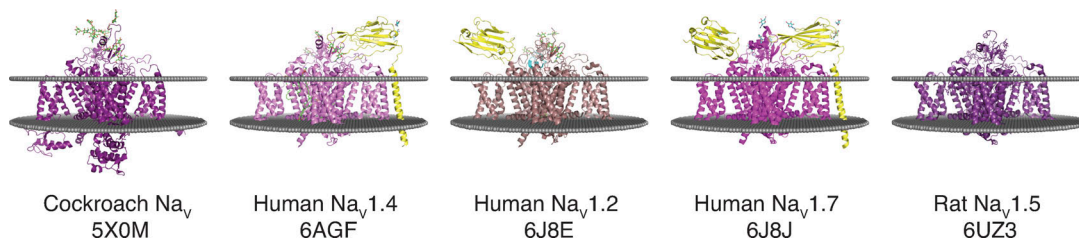


Figure 3. **Cryo-EM structures of NaVs.** α -Subunits are shown in purple and β -subunits are shown in yellow. 5X0M displays most of the N-terminal domain and the EFL of the CT domain.

CT helix α VI could correspond to distinct functional states of the channel.

Using structural alignments and protein engineering, Payandeh and coworkers postulated that deactivated VSD4 interactions with the EFL explain the electromechanical mechanism of fast inactivation (Clairfeuille et al., 2019). A VSD4- Na_VPaS chimera—VSD4 and DI-S5 of Na_VPaS swapped with the corresponding residues from $\text{Na}_V1.7$ —displays a conformation typical of VSD4 in an activated channel as visualized at 0 mV membrane potential. On the other hand, the VSD4- Na_VPaS chimera bound to the scorpion toxin (PDB accession no. 6NT3) displays a channel where S4 translates ~ 13 Å, trapping VSD4 in a deactivated conformation (Clairfeuille et al., 2019). The positive charges of the VSD4 S4 helix and S4-S5 linker interact with a negative conserved patch in the α I helix of the CT. This electrostatic interaction, termed switch 1, restrains the CT and, in turn, leads to switch 2 in which the DIII-DIV linker binds to a helix of the EFL and DIV-S6. Furthermore, $\text{Na}_V1.5$ charge-reversing mutations of the negatively charged EFL helix α I residues that bind VSD4 charges K7 and R8 display an enhanced steady-state inactivation and fast inactivation.

Electrophysiologic evidence for Ca^{2+} -dependent inactivation (CDI)

CDI results in enhanced inactivation of the voltage-gated channel and rapid reduction of the peak conductance when the Ca^{2+} concentration is increased. CDI was first described in cardiac L-type Ca^{2+} channels and represents an important negative feedback element in a wide spectrum of biologic contexts (Brehm and Eckert, 1978; Ben-Johny and Yue, 2014). While both

$\text{Na}_V1.4$ and $\text{Na}_V1.5$ bind CaM and have homologous CTs, intriguingly, only $\text{Na}_V1.4$ exhibits CaM-mediated CDI (Ben-Johny et al., 2014).

The role of the CT in CDI was demonstrated by exchanging the CT of the two channels; i.e., creating and expressing chimeric channels, $\text{Na}_V1.5$ -CT $\text{Na}_V1.4$ and $\text{Na}_V1.4$ -CT $\text{Na}_V1.5$ (Ben-Johny et al., 2014). Equivalent electrophysiologic measurements with these channels show that CDI takes place only with variants containing CT $\text{Na}_V1.4$ (Fig. 5, a and b). The conditions of the experiment were designed to closely mimic biologic conditions of Ca^{2+} signaling; chelated intracellular Ca^{2+} was rapidly released to a concentration of ~ 10 μM .

Determination of relevant binding affinities

Ca^{2+} sensing by CaM. Evans and Shea (2009) measured the dissociation constants of Ca^{2+} binding to CaM to reveal that, considering four possible free Ca^{2+} -CaM species (apo-CaM, $(\text{Ca}^{2+})_{2N}$, $(\text{Ca}^{2+})_{2C}$, and $(\text{Ca}^{2+})_4$ -CaM), only three species exist with significant abundance; the species with Ca^{2+} only in the N-lobe does not get populated because, given the low affinity of the N-lobe for Ca^{2+} , when it binds Ca^{2+} the C-lobe is already fully occupied.

Thermodynamic Na_V regulation by CaM. The affinity of CaM for cytoplasmic regions of the Na_V channels in the presence and absence of Ca^{2+} has been determined by multiple groups. The studies focus on two regions in particular: the DIII-DIV linker (forming the inactivation gate that modulates fast inactivation) and the CT containing the IQ motif. CaM affinities for short peptides of the inactivation gate (≤ 30 amino acids) are in the low micromolar range, e.g., Ca^{2+} -CaM with a K_d of 2.98 μM (Shah et al., 2006; Potet et al., 2009; Sarhan et al., 2012). The use of an extended sequence with two potential adjacent sites displays high affinity with a K_d of 12 nM (Johnson et al., 2018).

Numerous studies have also reported CaM interacting with the $\text{Na}_V1.5$ IQ domain. Shah and Chazin used intrinsic tyrosine fluorescence of CaM to show that an IQ motif-containing peptide of $\text{Na}_V1.5$ binds apo-CaM with ~ 160 nM K_d and Ca^{2+} -CaM with 2 μM K_d . Sarhan obtained similar values by using isothermal titration calorimetry (Shah et al., 2006; Sarhan et al., 2012). Moreover, the NMR chemical shift differences of apo-CaM with the $\text{Na}_V1.2$ IQ domain peptide, $\text{Na}_V1.1$ IQ, $\text{Na}_V1.6$ IQ, and $\text{Na}_V1.7$ IQ show perturbed resonances only in the CaM C-lobe. Extending these findings to all isoforms supports the premise that the apo-C-lobe is the primary partner of the Na_V CT (Isbell et al., 2018).

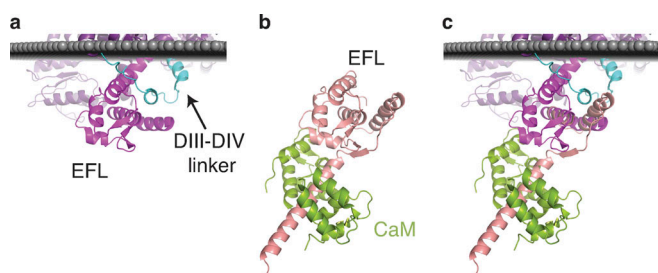


Figure 4. **Alignment of transmembrane Na_VPaS with CT $\text{Na}_V1.5$.** (a) Na_VPaS (PDB accession no. 5X0M) with cytoplasmic domain resolution. DIII-DIV linker is shown in cyan and EFL of CT in purple. (b) CT $\text{Na}_V1.5$ is shown in pink and apo-CaM in green (PDB accession no. 4OVN). (c) Alignment of Na_VPaS with CT $\text{Na}_V1.5$ shows overlap between the two structures (0.39 RMSD over 69 amino acids).

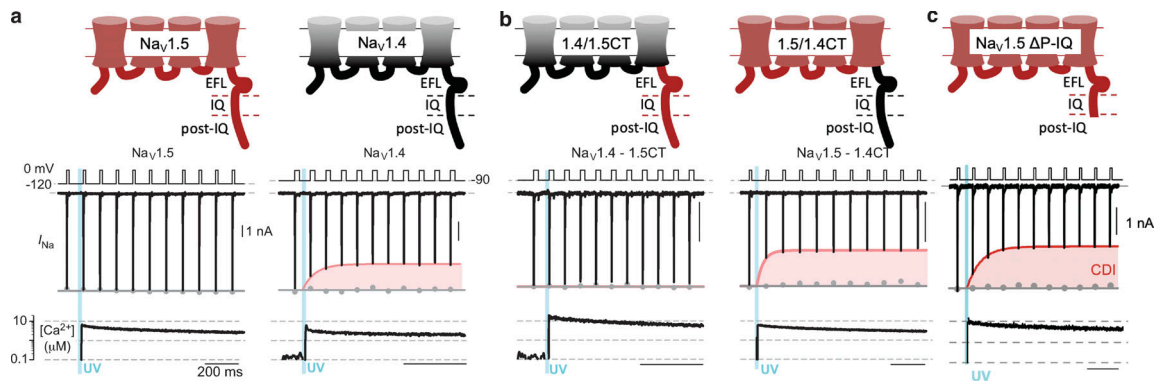


Figure 5. **Nav1.4 displays CDI.** (a) Nav1.5 Na⁺ current does not change upon Ca²⁺ release, but Nav1.4 I_{Na} is reduced upon optical Ca²⁺ release, indicated with a blue line. (b) When CTNav1.4 is transplanted to Nav1.5 and vice versa, the CDI still only takes place in channels with CTNav1.4. (c) Deletion of the Nav1.5 post-IQ motif reveals CDI with I_{Na} reduced at 10 μM Ca²⁺. a and b are adapted from Ben-Johny et al. (2014), and c is adapted from Yoder et al. (2019).

In all cases, apo-CaM shows the highest affinity of CaM species for CTNav_V compared with the Ca²⁺-containing species. Isothermal titration calorimetry experiments, adding 1 μM Ca²⁺ to the titration with WT CaM (four Ca²⁺ bound), has a strikingly different effect on the two isoforms: it lowers the affinity of CTNav_V1.4 by a factor of ~16 (K_d 17 nM versus 275 nM) and CTNav_V1.5 by only a factor of ~2 (K_d 48 nM versus 89 nM; Yoder et al., 2019). Yoder also determined binding of the species with Ca²⁺ occupied by individual CaM lobes by using CaM mutants that disable Ca²⁺ binding to both N-lobe sites or both C-lobe sites. The affinities of these mutants show marked differences between the two Nav_V isoforms. While both have high affinities when CaM N-lobes have bound Ca²⁺ ((Ca²⁺)_{2N}-CaM₃₄), the affinity of the Nav1.5 isoform for the (Ca²⁺)_{2C}-CaM₁₂ (3.6 μM) has a significantly higher K_d than that of Nav1.4 (154 nM). This difference has a major role in the CDI response of the channels.

Estimation of the fractional populations

To estimate the populations of the species participating in CDI, two equilibria have to be considered: binding of Ca²⁺ to CaM and binding of the different Ca²⁺-CaM species to CTNav_V. The fractional populations of Ca²⁺ and the four CaM species can be obtained using the affinities determined by Evans and Shea (Evans and Shea, 2009; Evans et al., 2011; Yoder et al., 2019). With the Ca²⁺ binding K_d s and the K_d s describing the binding affinity of CTNav_Vs to CaM in the presence or absence of Ca²⁺, the populations of the Nav_Vs bound with the different Ca²⁺-CaM states can be calculated (Fig. 6; Yoder et al., 2019). The most noteworthy difference between the behavior of the two isoforms, Nav1.4 and Nav1.5, is the presence of a significant population of Nav1.4 complexes with Ca²⁺ bound only to the CaM C-lobe. That is, while CTNav1.4 binds the Ca²⁺-occupied CaM C-lobe without binding the CaM N-lobe, CTNav1.5 binds the CaM N-lobe and the CaM C-lobe when the Ca²⁺ concentration increases. The fractional populations of the species present at 10 μM CaM (Fig. 6) show a difference in behavior of the two isoforms. An important distinction here is that functional Nav1.4 regulation relies largely on Ca²⁺ binding to the N-lobe of CaM, as coexpression of mutant CaM with EF hands 1 and 2 in the N-lobe disables dynamic Ca²⁺ regulation, while preventing Ca²⁺ binding to EF

hands 3 and 4 in the C-lobe largely spares CDI. Mechanisms that give rise to this divergent behavior between functional channel regulation and apparent Ca²⁺ sensitivity of the isolated Nav1.4CT-CaM complex are as yet unknown. One possibility is that additional Ca²⁺-CaM binding sites may be involved in triggering dynamic Ca²⁺ regulation of Nav1.4 channels.

Structures of the Ca²⁺-bound species

At low [Ca²⁺], the C-lobe of apo-CaM binds to CTs of the Nav1.4 (PDB accession no. 6MBA) and Nav1.5 (PDB accession no. 4OVN) at the IQ motif while the N-lobe interacts with the EFL. Under Ca²⁺-saturating conditions, the structures show that while the CaM C-lobe remains bound to the IQ motif, the N-lobe is found in different positions depending on the isoform and the conditions. This CaM property strongly suggests that the movement of the N-lobe and its choice of binding partner underly the signaling of different channel states depending on cellular context. The difference in CDI between the two isoforms appears to be explained by examining the Ca²⁺-containing structures found in PDB accession nos. 4JQO and 6MC9 (Wang et al., 2014; Yoder et al., 2019). Although the structure of PDB accession no. 4JQO was determined to 3.84-Å resolution with only 45% complete data and bound FHF1b, an inhibitor of the channel, it shows a state of the CaM N-lobe that provides a framework for understanding the functional data of Ca²⁺ and CaM regulation of Nav1.5. In this structure, the CaM N-lobe binds the long helix αVI of the CTNav1.5 at a sequence past the IQ-motif (post-IQ). This arrangement renders the Ca²⁺-bound N-lobe unable to interact with other regions of the channel. In contrast, at high [Ca²⁺], the CaM N-lobe interacts only weakly with CTNav1.4 and not with helix αVI. Its hydrophobic cleft is open and unoccupied in a way that would allow it to interact with other cytoplasmic regions of the channel, such as the DIII-DIV, and cause CDI.

The post-IQ region is likely responsible for the distinct behavior of the two isoforms. Notably, the need for the post-IQ motif for CDI was demonstrated by showing that, in the absence of the post-IQ (Δpost-IQ), Nav1.5 exhibits robust CDI (Fig. 5 c; Yoder et al., 2019). An alignment of the post-IQ sequences of the human Nav_V isoforms is shown in Fig. 7. In the case of interactions of the Ca²⁺-occupied CaM N-lobe, the main difference

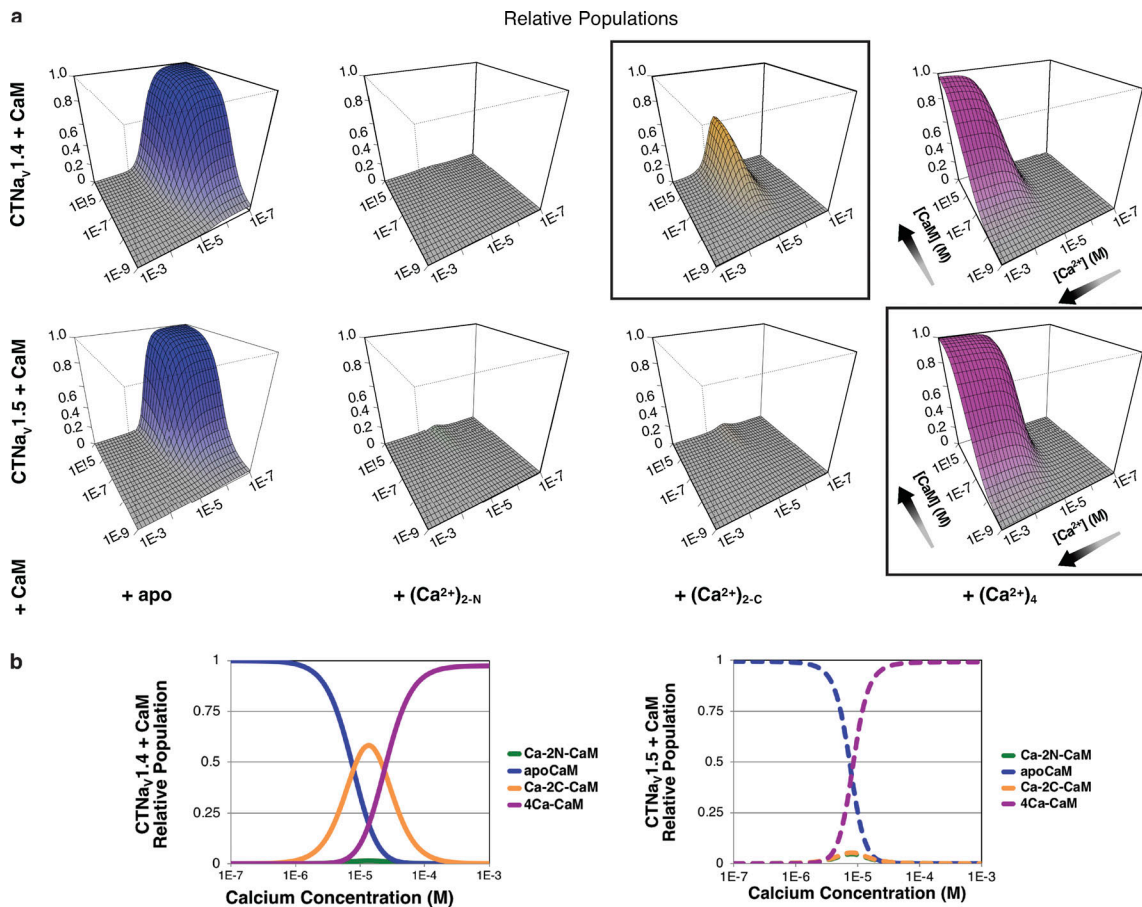


Figure 6. **Populations of CTNAV1.4 and CTNAV1.5 with bound CaM.** (a) Panels show the relative population (z-axis) of four CaM species bound to CTNAV, as a function of Ca²⁺ and CaM concentration. Black boxes indicate the dominant species at high CaM and 10 μM Ca²⁺; (Ca²⁺)_{2C}-CaM for CTNAV1.4 (top) and (Ca²⁺)₄-CaM for CTNAV1.5 (bottom). (b) Cross-section showing populations of CTNAV (Ca²⁺)-CaM species as a function of [Ca²⁺] at a [CaM] of 10 μM. Note the dramatic reduction of (Ca²⁺)_{2C}-CaM for CTNAV1.5 compared with CTNAV1.4. Adapted from Yoder et al. (2019).

seems to reside in the substitution of Nav1.5-Leu_1921 by a methionine Nav1.4-Met_1747. Nav1.5-Leu_1921 makes contact (4.7 Å) with Met_73 of the CaM N-lobe. Replacing Nav1.5-Leu_1921 with methionine in Nav1.4 results in possible conformations that either eliminate the interaction or produce clashes with CaM-Met_73 or with Ala_16. It remains to be determined what significant differences in other isoforms are responsible, at least in part, for the isoform-specific behavior of the channels. In any case, the importance of the post-IQ motif in the cytoplasmic regulation of the channels cannot be underestimated.

Intriguingly, CTNAV1.5 in complex with Ca²⁺-CaM and in the absence of FHF (PDB accession no. 6MUD; Gardill et al., 2019) displays an extended CaM conformation (with the N-lobe unbound) different from that of CTNAV1.5-CaM in the absence of Ca²⁺ (PDB accession no. 4OVN; CaM N-lobe bound to the EFL) or in the presence of both Ca²⁺ and FHF (PDB accession no. 4JQO; N-lobe bound post-IQ). 6MUD displays another CaM conformation, probably similar to that of CaM in 4DCK. This is likely a reflection of the flexibility of CaM, which can by itself adopt a very large number of conformations depending on the specific

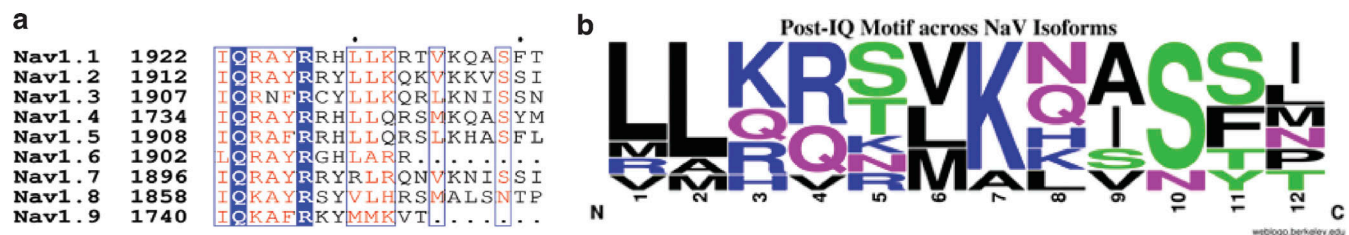


Figure 7. **Sequence alignment of the post-IQ sequence in the Nav1s.** (a) Alignment of the IQ and the post-IQ domains of the nine major human Nav isoforms. (b) Logo of the post-IQ sequences where the frequency of an amino acid at a given position is proportional to the size of its single amino acid letter descriptor.

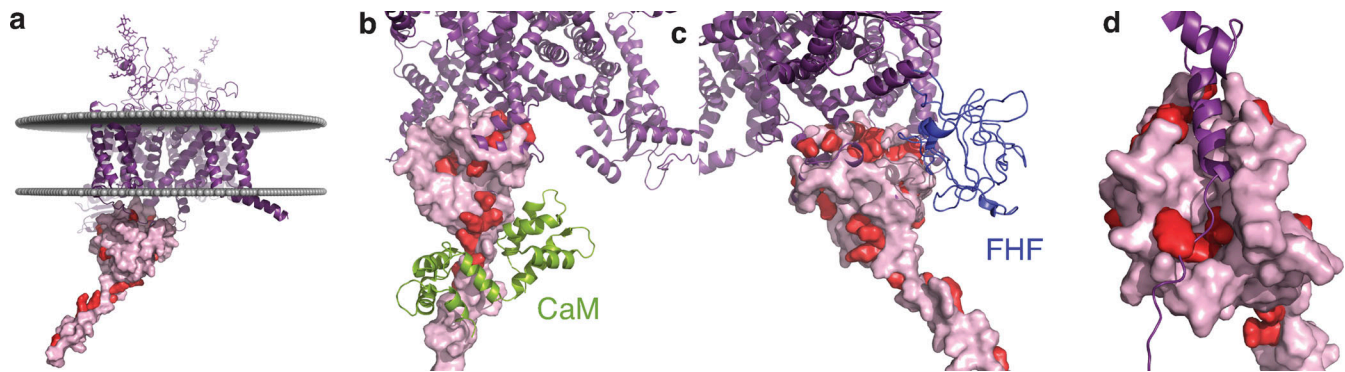


Figure 8. **Mutations in Nav1.5 mapped to its structure.** (a) Overall structure of Nav1.5 with the transmembrane portion as observed in the cryo-EM structure (PDB accession no. 6UZ3) in purple. CT domain as observed in PDB accession no. 4OVN, shown in pink surface with mutations displayed in red. (b) Zoom-in showing mutations in the EFL and IQ region, potentially interacting with (or in close proximity to) CaM. (c) Mutations interacting with FHF of PDB accession no. 4JQO. (d) Mutations of Nav1.5 in the EFL that line the binding site of the DIII-DIV linker.

conditions used in the structure determination. Being bound to the post-IQ can be considered to be a strong indication of specificity.

Channelopathies

The information about clinical aspects of Nav mutations is present in public databases such as ClinVar (<https://www.ncbi.nlm.nih.gov/clinvar>) and OMIM (<https://www.ncbi.nlm.nih.gov/omim>). Additionally, the International Union of Basic and Clinical Pharmacology-Database developed a database that includes pharmacologic and proteomic data, and a more recent paper compiled molecular and cellular data on Nav mutations that included patient phenotypic mutations as well as probes for the study of Navs (<https://www.nextprot.org/portals/navmut>; Hinard et al., 2017).

Alignment of x-ray crystallographic studies of CTNav1.5 and cryo-EM studies of the rat Nav1.5 allow us to map most of the mutations in the CT as well as in the DIII-DIV linker (Fig. 8 a). Interestingly, many mutations are at protein-protein interfaces, such as DIII-DIV with EFL, EFL-FHF, CTNav1.5-CaM, and CTNav1.5-NEDD4L, highlighting the exquisite regulation of the channel by its channel interacting proteins (Fig. 8, b-d). Mutations in SCN5A, the gene encoding Nav1.5, commonly lead to cardiac arrhythmias, including Brugada syndrome (a loss-of-function phenotype characterized by a decrease in the upstroke velocity of the action potential) and long-QT syndrome type III (LQT3; a gain-of-function phenotype resulting in delayed repolarization due to increased late Na current). Multiple cohorts of patients with irritable bowel syndrome have also shown a 2-3% prevalence of SCN5A mutations and coding polymorphisms resulting in abnormal electrophysiology as characterized in human embryonic kidney patch-clamp experiments (Saito et al., 2009; Beyder et al., 2014; Strege et al., 2018).

Of note, severe sinus bradycardia was observed in a patient with compound heterozygosity in the SCN5A gene (Nof et al., 2019). Specifically, mutations were observed in the DIII-DIV linker (Nav1.5_{K1493del}) and in helix α VI (Nav1.5_{A1924T}). The deletion of K1493 in the proximal DIII-DIV linker attenuates Nav1.5 expression by ~40% but was shown not to affect trafficking to

the plasma membrane (Nof et al., 2019). Nav1.5_{K1493del} altered gating properties of coexpressed functional Nav1.5 in a Ca²⁺- and Nav β 1-dependent manner. Intriguingly, Ben-Johny et al. (2014) determined that Nav1.4 displays rapid CDI but Nav1.5, when recombinantly expressed or in native muscle cells, does not. Moreover, the authors determined that CTNav1.4 governs CDI. In a critical experiment, they showed that the chimera of Nav1.5, with its CT replaced by CTNav1.4, displays CDI even though the rest of the channel has the Nav1.5 sequence. One possible difference between the experiments of the two laboratories is that the experiments of Ben-Johny and colleagues were done in the absence of Nav β 1, while the expression by Nof and colleagues was done in its presence (Nof et al., 2019). Structural analysis suggests that K1493del leads to changes in the protein conformation that will prevent the interaction of the DIII-DIV linker with the EFL helix since the equivalent residue of cockroach channel is part of the helix that sits between helix α I and α IV of the EFL. The associated mutation, A1924T, a post-IQ residue (Gabelli et al., 2014; Nof et al., 2019), impairs the Ca²⁺-dependent Nav β 1 modulation characterized in Nav1.5 WT currents (Nof et al., 2019). Nav1.5_{A1924T} is at the interface with CaM described in the complex structure CTNav1.5-CaM-Ca²⁺ (PDB accession no. 4JQO; Wang et al., 2014). Notably, a Ca²⁺-dependent Nav β 1 modulation that was characterized in Nav1.5_{WT} currents was impaired in the Nav1.5_{A1924T} variant.

LQT3 mutations Nav1.5_{Q1909R} (Tester and Ackerman, 2005; Tester et al., 2005) and Nav1.5_{R1913H} (Napolitano et al., 2005) are at the interface with CaM. Both were shown to result in increased late Na⁺ current. A mutant in the IQ motif that anchors CaM binding, Nav1.5_{Q1909R}, shows a depolarizing shift in steady-state inactivation, while Nav1.5_{Q1909A} destabilizes CaM binding. In addition, disruption of apo-CaM binding to Nav1.5 has been shown to upregulate persistent Na⁺ current. Furthermore, CaM overexpression reverses the increase in persistent Na⁺ current (Yan et al., 2017). This effect has been proposed to be mediated through an interaction between the DIII-DIV linker and CT (Gardill et al., 2018; Gade et al., 2020; Peters et al., 2020).

FHF2 is known to promote long-term inactivation of Nav channels (Liu et al., 2003; Dover et al., 2010; Savio-Galimberti

et al., 2012). Alignment of the EFL domains of the structures $\text{Na}_v1.5$ in the presence and absence of Ca^{2+} and FHF2 shows that the relation between helix αVI and the EFL domain is different between the two structures: the helix is rotated by $\sim 90^\circ$. This change is emphasized in the structures displayed in Fig. 2 b. In this case, the CaM C-lobe and Na_v helix αVI are aligned and, consequently, the EFL is the one showing the $\sim 90^\circ$ rotation (Wang et al., 2014). Mutations $\text{Na}_v1.5_{\text{L1896V}}$, $\text{Na}_v1.5_{\text{D1839G}}$ (Kapplinger et al., 2009), and $\text{Na}_v1.5_{\text{R1897W}}$ (Kapplinger et al., 2009) form a shallow cavity at the interface with the loop of FHF2 spanning residues 95–99. $\text{Na}_v1.5_{\text{E190IN}}$ (Kapplinger et al., 2009) and $\text{Na}_v1.5_{\text{S1904L}}$ (Bankston et al., 2007; Kapplinger et al., 2009) mutations, also at the FHF2 interface, are involved in the switch that helix αVI forms by rotating 90° with respect to the EFL, suggesting a possible mode of signaling that mediates long-term inactivation. Interestingly, FHF1 coexpression also prevents rapid Ca^{2+} -dependent regulation of $\text{Na}_v1.4$ channels, suggesting that there may be crosstalk between CaM and FHF regulatory mechanisms (Niu et al., 2018). Structurally, as FHF interacts upstream of the Na_v IQ domain, one possibility is that FHF uncouples distal conformational changes elicited by CaM, thereby preventing dynamic Ca^{2+} regulation.

Mutations in the EFL $\text{Na}_v1.5_{\text{A1780D}}$ (Beyder et al., 2014), $\text{Na}_v1.5_{\text{I782V}}$, $\text{Na}_v1.5_{\text{E1784K}}$ (Wei et al., 1999), $\text{Na}_v1.5_{\text{L1786N}}$, $\text{Na}_v1.5_{\text{Y1795C}}$ (Rivolta et al., 2001), $\text{Na}_v1.5_{\text{W1798X}}$, $\text{Na}_v1.5_{\text{M1851V}}$ (Han et al., 2018), and $\text{Na}_v1.5_{\text{M1875T}}$ line the cavity that EFL helices αI and αIV form where the DIII–DIV linker binds. $\text{Na}_v1.5_{\text{A1780D}}$ (Beyder et al., 2014), observed in irritable bowel syndrome patients, displays faster inactivation than WT, while $\text{Na}_v1.5_{\text{M1851V}}$ (Kehl et al., 2004; Han et al., 2018) displays slower inactivation and has a faster recovery from inactivation. Mutation $\text{Na}_v1.5_{\text{E1784K}}$, and other neutralizing mutations of the acidic residues of helix αI have been observed (Jones and Ruben, 2008). Charge reversal of EFL $\text{Na}_v1.5_{\text{D1789K}}$, $\text{Na}_v1.5_{\text{D1792K}}$, and $\text{Na}_v1.5_{\text{E1796K}}$ display ~ 8 mV left shift in steady-state inactivation as well as faster inactivation (Clairfeuille et al., 2019). The presence of underlying arrhythmia mutations in these residues strengthens the hypothesis that they are involved in an electrostatic bridge with the positive charges of S4 (Clairfeuille et al., 2019) that cause fast inactivation. Interestingly, mutations at Y1795 have two different functional consequences. While Y1795H underlies Brugada syndrome, Y1795C underlies LQT3 syndrome (Rivolta et al., 2001). In both cases, the channels have gating defects. While the cysteine mutant channels inactivate more slowly, the histidine mutations display a reduction in peak current density. Structurally, these mutations sit at the EFL cavity where the DIII–DIV helix is predicted to bind (Fig. 8 d).

The skeletal muscle channelopathies due to mutations in *SCN4A*, the gene that encodes $\text{Na}_v1.4$, are rare diseases. Muscle excitability can be pathologically enhanced or depressed due to $\text{Na}_v1.4$ mutations and produce skeletal muscle phenotypes, such as myotonia, periodic paralysis, myasthenia, and myopathy. Muscle stiffness, myotonia, is due to gain-of-function hyperexcitability. On the other hand, reduced excitability results in a transient or chronic state of weakness. These clinical phenotypes correlate with sustained depolarization of the resting potential, rendering muscle fibers electrically nonexcitable (Cannon, 2018). The reduced muscle

tone of congenital myopathy and neonatal hypokinesia has also been described (Zaharieva et al., 2016). By using the cryo-EM structure of $\text{Na}_v1.4$ (PDB accession no. 6AGF) and the $\text{CTNa}_v1.4$ complex with CaM (PDB accession no. 6MBA), we mapped some of the mutations (Fig. 9).

Specifically, patients with paramyotonia congenita (PMC) display mutations in the proximal DIII–DIV linker $\text{Na}_v1.4_{\text{G1306E}}$ (Singh et al., 2014), $\text{Na}_v1.4_{\text{T1313M}}$ (Matthews et al., 2011). Mechanistically, it is a consistent correlation that mutations in the DIII–DIV linker—the inactivation gate—result in gain of function due to abnormal fast inactivation. Unlike with $\text{Na}_v1.5$, we did not find any published mutations in the distal DIII–DIV linker. The myotonia mutation $\text{Na}_v1.4_{\text{Q1633E}}$ and PMC mutation $\text{Na}_v1.4_{\text{F1705I}}$ (Wu et al., 2005) are both mapped to the EFL helix αIV . Similar to $\text{Na}_v1.5$, the $\text{Na}_v1.4$ EFL helices αI and αIV form the binding site for the DIII–DIV linker. These myotonia and PMC mutations show a slower rate of fast inactivation, causing hyperexcitability (Singh et al., 2014). Structural alignment of $\text{CTNa}_v1.4$ with $\text{CTNa}_v1.5$ –FHF suggests that $\text{Na}_v1.4_{\text{E1702K}}$ (Miller et al., 2004) could be at the interface of $\text{Na}_v1.4$ –FHF (Fig. 9 b). This interaction is speculative thus far, as the field lacks investigation into potential FHF regulation of $\text{Na}_v1.4$. Interestingly, both mutations also reduced Ca^{2+} regulation of $\text{Na}_v1.4$ channels (Ben-Johny et al., 2014). Recent work has shown that Ca^{2+} release from the RYR in skeletal muscle inhibits native $\text{Na}_v1.4$ currents. This reduction in Na^+ current may be a physiologically relevant, activity-dependent feedback mechanism that prevents excess muscle contraction during periods of repetitive activity (Sarbjit-Singh et al., 2020). Consequently, disruption of CDI by channelopathic mutations may be a contributing factor for debilitating myotonias.

Dimerization of Na_v channels

It has been the paradigm of the functioning of Na_v channels that the individual molecules do not oligomerize and fire independently; however, this interpretation is being challenged by new experiments and revisions of old data. Here, we will review this evidence, especially with reference to structural data that show that two α -subunits can interact to form a dimer.

Starting several decades ago, investigators presented data that supported a mechanism that involved the coupled gating by two or more Na_v s. For example, Catterall and Morrow (1978), using saxitoxin-treated neuroblastoma cells, found that when channels open and close the probability of two or three opening together is much higher than that of the single channels. One tentative explanation was that opening is favored by cooperative interactions between channels. Aldrich et al. (1983) similarly observed a higher incidence of even numbers of channels under the patch in their single-channel recordings. In another study, Naundorf et al. (2006) argued that in cortical neurons the details of the dynamics of the action potential initiation are more compatible with cooperativity among channels than with the channels firing independently, as the stoichiometry of the Hodgkin–Huxley-style models did not justify the sharp action potential initiation. Using the ischemic metabolite lysophosphatidylcholine, Undrovinas et al. (1992) observed two to three synchronized channel openings, while no single openings were reported.

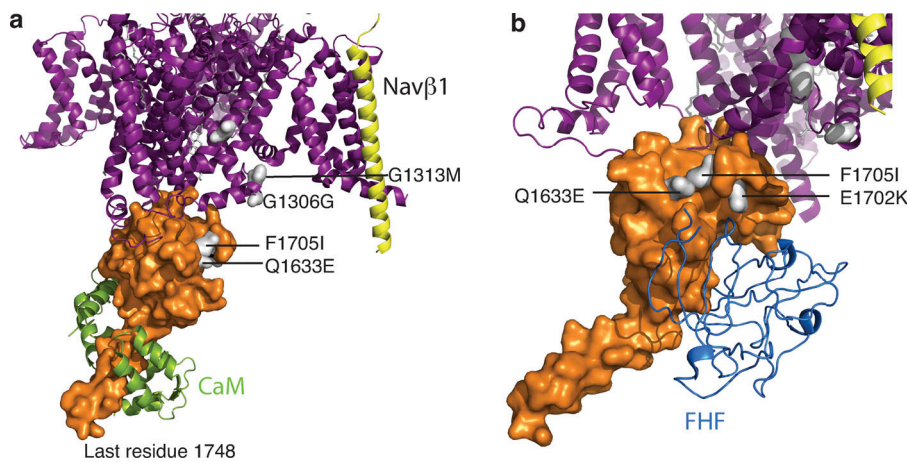


Figure 9. Mutations in Nav_v1.4 mapped to its structure. (a) Overall structure of Nav_v1.4 with the transmembrane portion as observed in the cryo-EM structure (PDB accession no. 6AGF) in purple and Nav_v β1 in yellow. CT domain as observed in PDB accession no. 6MBA, shown in orange surface with mutations displayed in white. (b) Different 6MBA Nav_v1.4 orientation with FHF (from PDB accession no. 4JQO of Nav_v1.5 with FHF1b; aligned to 6MBA by CTNav_v EFL) to show a possible interaction with Q1633.

An independent indication of interaction between Nav_v α-subunits is provided by the existence of dominant-negative mutants (Clatot et al., 2018). A comprehensive study of Nav_v1.5 using a variety of techniques, including coimmunoprecipitation and chemical cross-linking, showed the existence of Nav_v1.5 dimers (Clatot et al., 2017). This study concluded that, not only do α-subunits dimerize, but assembling as dimers results in coupled gating. Using N-terminal deletion mutants of Nav_v1.5, the study showed that dimerization of α-subunits requires residues 493–517. These residues are part of the cytoplasmic extension of the long α-helix S6 of DI, which is part of the unstructured loop connecting DI to DII. Clatot et al. (2017) also showed that removal of the CT did not hamper Nav_v-Nav_v interaction, which suggests that any possible CT-CT interaction would be dependent on a different driver of Nav_v-Nav_v interaction.

In human embryonic kidney cells, the polymorphism H558R (DI-DII linker) restores WT SCN5A current from the gain-of-function P2006A mutation when expressed in the same channel as well as when coexpressed in separate channels, further supporting the interaction of the DI-DII linker with the CT (Shinlapawittayatorn et al., 2011). No experimental evidence shows, however, that the DI-DII loop is the only region of the channel involved in dimerization. The DIII-DIV loop (residues 1467–1529) and the CT (residues 1776–2016), both in the cytoplasmic side of the membrane, are long regions that were shown to participate in some aspects of the regulation and control of the channel activity. With respect to Nav_v1.5-Nav_v1.5 dimerization, there is strong structural information that not only makes a case for channel-channel interaction, but also provides the structures of the interfaces (Gabelli et al., 2014).

Dimerization of the Nav_v1.5 requires interaction with 14-3-3, a protein of a family of conserved regulatory molecules that are expressed in all eukaryotic cells. 14-3-3 bind a large number of functionally diverse signaling proteins, including kinases, phosphatases, and transmembrane proteins (Allouis et al., 2006; Clatot et al., 2017). There are seven genes coding for 14-3-3 proteins that, when expressed, form homo- and heterodimers. Cross-linking and coimmunoprecipitation experiments of WT Nav_v1.5 and Nav_v1.5 deletion mutants with 14-3-3 provided the majority of the information about the formation of dimers and the location of the regions that interact in their formation.

Similar experiments were performed with the neuronal channels Nav_v1.1 and Nav_v1.2 (Clatot et al., 2017). Cross-linking and coimmunoprecipitation of Nav_v1.1 and Nav_v1.2 with 14-3-3 clearly showed the presence of dimers and single-channel experiments showed cooperative two-channel events extending the evidence of dimerization to at least two other isoforms.

The first structural report of a plausible Nav_v-Nav_v interaction was presented in the structure of a human CTNav_v1.5 fragment (1773–1929) in complex with apo-CaM (Gabelli et al., 2014). This crystal structure shows CT-CT interactions: the EFL domains (1773–1882) of each CTNav_v1.5 molecule contacts the CT portion of helix αVI (1910–1926) of another CTNav_v1.5 molecule (Fig. 10). This CTNav_v1.5-CTNav_v1.5 interaction (buried area ~900 Å² with a complementarity index of 0.55 as calculated by PISA [proteins, interfaces, structures, and assemblies]) is mainly hydrophobic (Gabelli et al., 2014). Both values, that of buried area and of the complementarity index, although low, are still in the range observed for interfaces connecting components of an oligomer.

Interestingly, in the structure of the Nav_vPas, the first helix of the DIII-DIV loop binds to the EFL of the same molecule (Shen et al., 2017). This observation indicates that, despite the fact that the EFL does not bind Ca²⁺, it does have the ability to bind helices. There are differences, however, between the two arrangements of the EFL binding to the helix αVI or the DIII-DIV linker. First, although both helices—the helix αVI and the helix DIII-DIV loop—bind in the main groove of the EFL, they bind in opposite directions. Second, with the CT construct used in the crystal structure (residues 1773–1929), the end of helix αVI occupies only a fraction of the groove. It can be expected that a longer construct could bind to a larger portion of the groove, increasing the buried area. Significantly, the residues of helix αVI (1910–1926) that interact with the EFL of another molecule are all within the post-IQ motif (1910–1927). This interaction shows important specificity. Salt bridges bind the helix at both ends of the motif: Glu1804–Arg1910 and Glu1799–Arg1914, and Asp1792–Lys1922 at the other. Hydrogen bonds (Tyr1795–Arg1914 and Asn1883–Ser1920) are also important to stabilize the interaction. A αVI helix-EFL interaction was postulated by Chazin and coworkers (Chagot et al., 2009) and measured by transition-metal ion FRET (Glaaser et al., 2012), but it was interpreted as an intramolecular interaction and not as an interaction between two molecules.

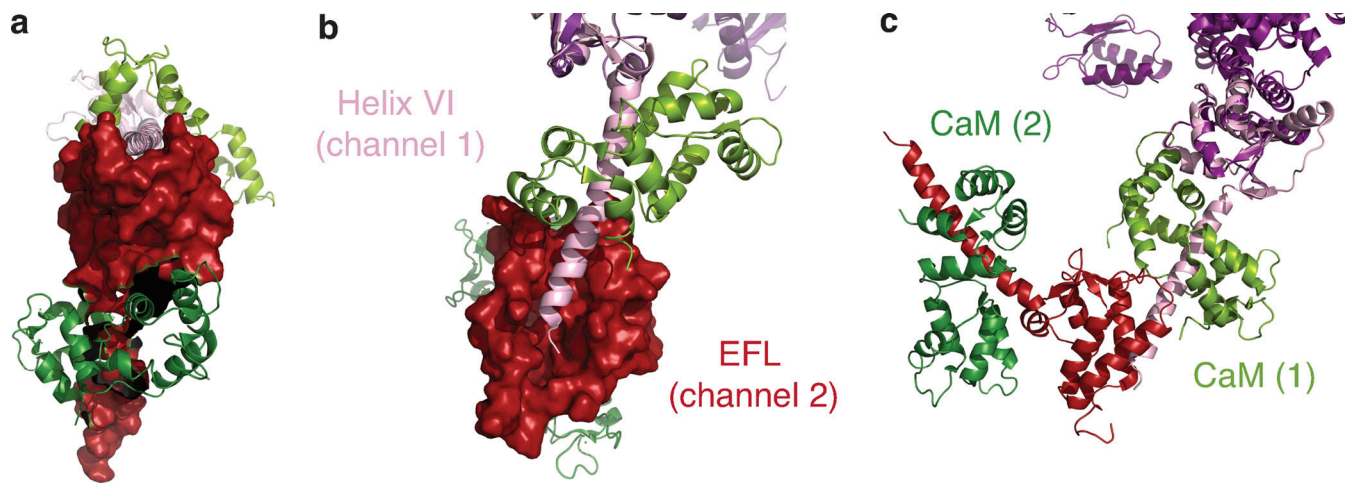


Figure 10. **Na_v-Na_v dimerization: interaction between CT helix α VI and EFL of an adjacent channel.** (a) Front view of the complex of CTNa_v1.5-CaM (red surface) with another channel's helix α VI (pink ribbons) as observed in PDB accession no. 4OVN. CaM bound to each channel is shown in shades of green. (b) Bird's eye view of a; the binding site of helix α VI of channel 1 (pink ribbons) on EFL of channel 2 (red surface). (c) Rotated 90° with both channels 1 and 2 shown in ribbons. Na_v1.5 channel 1 is shown in pink with its CaM (light green), and Na_v1.5 channel 2 EFL in red with its CaM (dark green).

For comparison, there are similarities and differences between Na_v1.5 and Na_v1.4. In the crystal structure of the CTNa_v1.4-Ca²⁺-CaM, the end of helix α VI also interacts with the EFL of another molecule. In this case, however, the interaction is with a symmetry-related molecule, and the residues of helix α VI are further along the helix, starting at residue 1742, past the beginning of the post-IQ motif (1734 in Na_v1.4; Yoder et al., 2019). Nevertheless, these and other observations challenge the present paradigm that Na_vs exist in complexes containing a single α -subunit.

Recent studies suggest that dimerization may have an effect in axonal impulse conduction and cell-cell adhesion in a way that could have consequences in multiple diseases (Agullo-Pascual et al., 2014; Freeman et al., 2016). This shift in paradigm—i.e., the channels assemble and fire as dimers—suggests a simple mechanism for dominant-negative mutants as well as for the coupling of the effect of Na_v mutants present in various channelopathies.

Conclusion

The investigations reviewed here highlight the importance of high-resolution structure in understanding the complex molecular architecture underlying cellular excitation. The recent cryo-EM structures of several Na_vs provided a wealth of information about the channel, but lacked information about the cytoplasmic CT, where cellular regulation of channel activity takes place. This gap was bridged with x-ray diffraction and NMR structures of the CT expressed as a soluble protein. CT-CT as well as CT-CaM and Ca²⁺ interactions were revealed by these structures. Structural studies of CaM N-lobe binding sites are enhanced by mutational studies pointing to the relevance for the β -subunit in Ca²⁺ regulation of Na_v1.5 as well as putative channel dimerization. These interactions may represent varying stages of channel activation or its cell type-specific regulation and are key in parsing the intriguing phenomenon of Ca²⁺ regulation of a Na⁺ channel.

Nathan et al.

Structural basis of cytoplasmic Na_v1.5 and Na_v1.4 regulation

Acknowledgments

Nestor Saiz served as guest editor.

This work was funded by National Institutes of Health, National Heart, Lung, and Blood Institute grant HL128743.

The authors declare no competing financial interests.

Authors contributions: conceptualization: S.B. Gabelli and L.M. Amzel; data curation: S. Nathan, J.B. Yoder, M. Ben-Johny, and S.B. Gabelli; formal analysis: S. Nathan and S.B. Gabelli; supervision: S.B. Gabelli, G.F. Tomaselli, M. Ben-Johny, and L.M. Amzel; writing – original draft: S. Nathan, S.B. Gabelli, and L.M. Amzel; visualizations: S. Nathan, J.B. Yoder, and M. Ben-Johny; writing – review and editing: S. Nathan, S.B. Gabelli, J.B. Yoder, L. Srinivasan, R.W. Aldrich, G.F. Tomaselli, M. Ben-Johny, and L.M. Amzel.

Submitted: 31 July 2020

Accepted: 6 November 2020

References

- Adelman, J.P. 2016. SK channels and calmodulin. *Channels (Austin)*. 10:1–6. <https://doi.org/10.1080/19336950.2015.1029688>
- Agullo-Pascual, E., X. Lin, A. Leo-Macias, M. Zhang, F.X. Liang, Z. Li, A. Pfenniger, I. Lübke, S. Keegan, D. Fenyő, et al. 2014. Super-resolution imaging reveals that loss of the C-terminus of connexin43 limits microtubule plus-end capture and Nav1.5 localization at the intercalated disc. *Cardiovasc. Res.* 104:371–381. <https://doi.org/10.1093/cvr/cvu195>
- Aldrich, R.W., D.P. Corey, and C.F. Stevens. 1983. A reinterpretation of mammalian sodium channel gating based on single channel recording. *Nature*. 306:436–441. <https://doi.org/10.1038/306436a0>
- Allouis, M., F. Le Bouffant, R. Wilders, D. Pérez, J.J. Schott, J. Noireaud, H. Le Marec, J. Mérot, D. Escande, and I. Baró. 2006. 14-3-3 is a regulator of the cardiac voltage-gated sodium channel Nav1.5. *Circ. Res.* 98: 1538–1546. <https://doi.org/10.1161/01.RES.0000229244.97497.2c>
- Bähler, M., and A. Rhoads. 2002. Calmodulin signaling via the IQ motif. *FEBS Lett.* 513:107–113. [https://doi.org/10.1016/S0014-5793\(01\)03239-2](https://doi.org/10.1016/S0014-5793(01)03239-2)
- Bankston, J.R., K.J. Sampson, S. Kateriya, I.W. Glaaser, D.L. Malito, W.K. Chung, and R.S. Kass. 2007. A novel LQT-3 mutation disrupts an inactivation gate complex with distinct rate-dependent phenotypic

- consequences. *Channels (Austin)*. 1:273–280. <https://doi.org/10.4161/chan.4956>
- Ben-Johny, M., and D.T. Yue. 2014. Calmodulin regulation (calmodulation) of voltage-gated calcium channels. *J. Gen. Physiol.* 143:679–692. <https://doi.org/10.1085/jgp.201311153>
- Ben-Johny, M., P.S. Yang, J. Niu, W. Yang, R. Joshi-Mukherjee, and D.T. Yue. 2014. Conservation of Ca²⁺/calmodulin regulation across Na and Ca²⁺ channels. *Cell*. 157:1657–1670. <https://doi.org/10.1016/j.cell.2014.04.035>
- Beyder, A., A. Mazzone, P.R. Strege, D.J. Tester, Y.A. Saito, C.E. Bernard, F.T. Enders, W.E. Ek, P.T. Schmidt, A. Dlugosz, et al. 2014. Loss-of-function of the voltage-gated sodium channel Nav1.5 (channelopathies) in patients with irritable bowel syndrome. *Gastroenterology*. 146:1659–1668. <https://doi.org/10.1053/j.gastro.2014.02.054>
- Brehm, P., and R. Eckert. 1978. Calcium entry leads to inactivation of calcium channel in Paramecium. *Science*. 202:1203–1206. <https://doi.org/10.1126/science.103199>
- Cannon, S.C. 2018. Sodium Channelopathies of Skeletal Muscle. *Handb. Exp. Pharmacol.* 246:309–330. https://doi.org/10.1007/164_2017_52
- Catterall, W.A., and C.S. Morrow. 1978. Binding to saxitoxin to electrically excitable neuroblastoma cells. *Proc. Natl. Acad. Sci. USA*. 75:218–222. <https://doi.org/10.1073/pnas.75.1.218>
- Chagot, B., and W.J. Chazin. 2011. Solution NMR structure of Apo-calmodulin in complex with the IQ motif of human cardiac sodium channel Nav1.5. *J. Mol. Biol.* 406:106–119. <https://doi.org/10.1016/j.jmb.2010.11.046>
- Chagot, B., F. Potet, J.R. Balsler, and W.J. Chazin. 2009. Solution NMR structure of the C-terminal EF-hand domain of human cardiac sodium channel Nav1.5. *J. Biol. Chem.* 284:6436–6445. <https://doi.org/10.1074/jbc.M807747200>
- Clairfeuille, T., A. Cloake, D.T. Infield, J.P. Llongueras, C.P. Arthur, Z.R. Li, Y. Jian, M.F. Martin-Eauclaire, P.E. Bougis, C. Ciferri, et al. 2019. Structural basis of α -scorpion toxin action on Na_v channels. *Science*. 363:eav8573. <https://doi.org/10.1126/science.aav8573>
- Clatot, J., M. Hoshi, X. Wan, H. Liu, A. Jain, K. Shinlapawittayatorn, C. Marionneau, E. Ficker, T. Ha, and I. Deschênes. 2017. Voltage-gated sodium channels assemble and gate as dimers. *Nat. Commun.* 8:2077. <https://doi.org/10.1038/s41467-017-02262-0>
- Clatot, J., Y. Zheng, A. Girardeau, H. Liu, K.R. Laurita, C. Marionneau, and I. Deschênes. 2018. Mutant voltage-gated Na⁺ channels can exert a dominant negative effect through coupled gating. *Am. J. Physiol. Heart Circ. Physiol.* 315:H1250–H1257. <https://doi.org/10.1152/ajpheart.00721.2017>
- Dover, K., S. Solinas, E. D'Angelo, and M. Goldfarb. 2010. Long-term inactivation particle for voltage-gated sodium channels. *J. Physiol.* 588:3695–3711. <https://doi.org/10.1113/jphysiol.2010.192559>
- Evans, T.I., and M.A. Shea. 2009. Energetics of calmodulin domain interactions with the calmodulin binding domain of CaMKII. *Proteins*. 76:47–61. <https://doi.org/10.1002/prot.22317>
- Evans, T.I., J.W. Hell, and M.A. Shea. 2011. Thermodynamic linkage between calmodulin domains binding calcium and contiguous sites in the C-terminal tail of Ca(V)₁L2. *Biophys. Chem.* 159:172–187. <https://doi.org/10.1016/j.bpc.2011.06.007>
- Feldkamp, M.D., L. Yu, and M.A. Shea. 2011. Structural and energetic determinants of apo calmodulin binding to the IQ motif of the Na(V)₁L2 voltage-dependent sodium channel. *Structure*. 19:733–747. <https://doi.org/10.1016/j.str.2011.02.009>
- Fotia, A.B., J. Ekberg, D.J. Adams, D.I. Cook, P. Poronnik, and S. Kumar. 2004. Regulation of neuronal voltage-gated sodium channels by the ubiquitin-protein ligases Nedd4 and Nedd4-2. *J. Biol. Chem.* 279:28930–28935. <https://doi.org/10.1074/jbc.M402820200>
- Freeman, S.A., A. Desmazières, D. Fricker, C. Lubetzki, and N. Sol-Foulon. 2016. Mechanisms of sodium channel clustering and its influence on axonal impulse conduction. *Cell. Mol. Life Sci.* 73:723–735. <https://doi.org/10.1007/s00018-015-2081-1>
- Gabelli, S.B., A. Boto, V.H. Kuhns, M.A. Bianchet, F. Farinelli, S. Aripirala, J. Yoder, J. Jakoncic, G.F. Tomaselli, and L.M. Amzel. 2014. Regulation of the Nav1.5 cytoplasmic domain by calmodulin. *Nat. Commun.* 5:5126. <https://doi.org/10.1038/ncomms6126>
- Gade, A.R., S.O. Marx, and G.S. Pitt. 2020. An interaction between the III-IV linker and CTD in Nav1.5 confers regulation of inactivation by CaM and FHF. *J. Gen. Physiol.* 152:e201912434. <https://doi.org/10.1085/jgp.201912434>
- Gardill, B.R., R.E. Rivera-Acevedo, C.C. Tung, M. Okon, L.P. McIntosh, and F. Van Petegem. 2018. The voltage-gated sodium channel EF-hands form an interaction with the III-IV linker that is disturbed by disease-causing mutations. *Sci. Rep.* 8:4483. <https://doi.org/10.1038/s41598-018-22713-y>
- Gardill, B.R., R.E. Rivera-Acevedo, C.C. Tung, and F. Van Petegem. 2019. Crystal structures of Ca²⁺-calmodulin bound to Nav_v C-terminal regions suggest role for EF-hand domain in binding and inactivation. *Proc. Natl. Acad. Sci. USA*. 116:10763–10772. <https://doi.org/10.1073/pnas.1818618116>
- Gavillet, B., J.S. Rougier, A.A. Domenighetti, R. Behar, C. Boixel, P. Ruchat, H.A. Lehr, T. Pedrazzini, and H. Abriel. 2006. Cardiac sodium channel Nav1.5 is regulated by a multiprotein complex composed of syntrophins and dystrophin. *Circ. Res.* 99:407–414. <https://doi.org/10.1161/01.RES.0000237466.13252.5e>
- Glaaser, I.W., J.D. Osteen, A. Puckerin, K.J. Sampson, X. Jin, and R.S. Kass. 2012. Perturbation of sodium channel structure by an inherited Long QT Syndrome mutation. *Nat. Commun.* 3:706. <https://doi.org/10.1038/ncomms1717>
- Goetz, R., K. Dover, F. Laezza, N. Shtraizent, X. Huang, D. Tchetchik, A.V. Eliseenkova, C.F. Xu, T.A. Neubert, D.M. Ornitz, et al. 2009. Crystal structure of a fibroblast growth factor homologous factor (FHF) defines a conserved surface on FHF for binding and modulation of voltage-gated sodium channels. *J. Biol. Chem.* 284:17883–17896. <https://doi.org/10.1074/jbc.M109.001842>
- Han, D., H. Tan, C. Sun, and G. Li. 2018. Dysfunctional Nav1.5 channels due to SCN5A mutations. *Exp. Biol. Med.* (Maywood). 243:852–863. <https://doi.org/10.1177/1535370218777972>
- Hinard, V., A. Britan, M. Schaeffer, M. Zahn-Zabal, U. Thomet, J.S. Rougier, A. Bairoch, H. Abriel, and P. Gaudet. 2017. Annotation of functional impact of voltage-gated sodium channel mutations. *Hum. Mutat.* 38:485–493. <https://doi.org/10.1002/humu.23191>
- Holm, A.N., A. Rich, S.M. Miller, P. Strege, Y. Ou, S. Gibbons, M.G. Sarr, J.H. Szurszewski, J.L. Rae, and G. Farrugia. 2002. Sodium current in human jejunal circular smooth muscle cells. *Gastroenterology*. 122:178–187. <https://doi.org/10.1053/gast.2002.30346>
- Hovey, L., C.A. Fowler, R. Mahling, Z. Lin, M.S. Miller, D.C. Marx, J.B. Yoder, E.H. Kim, K.M. Tefft, B.C. Waite, et al. 2017. Calcium triggers reversal of calmodulin on nested anti-parallel sites in the IQ motif of the neuronal voltage-dependent sodium channel Nav1.2. *Biophys. Chem.* 224:1–19. <https://doi.org/10.1016/j.bpc.2017.02.006>
- Isbell, H.M., A.M. Kilpatrick, Z. Lin, R. Mahling, and M.A. Shea. 2018. Backbone resonance assignments of complexes of apo human calmodulin bound to IQ motif peptides of voltage-dependent sodium channels Nav1.1, Nav1.4 and Nav1.7. *Biomol. NMR Assign.* 12:283–289. <https://doi.org/10.1007/s12104-018-9824-5>
- Jo, T., T. Nagata, H. Iida, H. Imuta, K. Iwasawa, J. Ma, K. Hara, M. Omata, R. Nagai, H. Takizawa, et al. 2004. Voltage-gated sodium channel expressed in cultured human smooth muscle cells: involvement of SCN9A. *FEBS Lett.* 567:339–343. <https://doi.org/10.1016/j.febslet.2004.04.092>
- Johnson, C.N., F. Potet, M.K. Thompson, B.M. Kroncke, A.M. Glazer, M.W. Voehler, B.C. Knollmann, A.L. George Jr., and W.J. Chazin. 2018. A Mechanism of Calmodulin Modulation of the Human Cardiac Sodium Channel. *Structure*. 26:683–694.e3. <https://doi.org/10.1016/j.str.2018.03.005>
- Jones, D.K., and P.C. Ruben. 2008. Biophysical defects in voltage-gated sodium channels associated with long QT and Brugada syndromes. *Channels (Austin)*. 2:70–80. <https://doi.org/10.4161/chan.2.2.6000>
- Kaplinger, J.D., D.J. Tester, B.A. Salisbury, J.L. Carr, C. Harris-Kerr, G.D. Pollevick, A.A. Wilde, and M.J. Ackerman. 2009. Spectrum and prevalence of mutations from the first 2,500 consecutive unrelated patients referred for the FAMILION long QT syndrome genetic test. *Heart Rhythm*. 6:1297–1303. <https://doi.org/10.1016/j.hrthm.2009.05.021>
- Kawasaki, H., and R.H. Kretsinger. 2012. Analysis of the movements of helices in EF-hands. *Proteins*. 80:2592–2600. <https://doi.org/10.1002/prot.24143>
- Kehl, H.G., W. Haverkamp, G. Rellensmann, T.M. Yelbuz, T. Krasemann, J. Vogt, and E. Schulze-Bahr. 2004. Images in cardiovascular medicine. Life-threatening neonatal arrhythmia: successful treatment and confirmation of clinically suspected extreme long QT-syndrome-3. *Circulation*. 109:e205–e206. <https://doi.org/10.1161/01.CIR.0000128874.43908.CA>
- Kovalevskaya, N.V., M. van de Waterbeemd, F.M. Bokhovchuk, N. Bate, R.J. Bindels, J.G. Hoenderop, and G.W. Vuister. 2013. Structural analysis of calmodulin binding to ion channels demonstrates the role of its plasticity in regulation. *Pflugers Arch.* 465:1507–1519. <https://doi.org/10.1007/s00424-013-1278-0>
- Lenaeus, M.J., T.M. Gamal El-Din, C. Ing, K. Ramanadane, R. Pomès, N. Zheng, and W.A. Catterall. 2017. Structures of closed and open states of a voltage-gated sodium channel. *Proc. Natl. Acad. Sci. USA*. 114:E3051–E3060. <https://doi.org/10.1073/pnas.1700761114>

- Liu, C.J., S.D. Dib-Hajj, and S.G. Waxman. 2001. Fibroblast growth factor homologous factor 1B binds to the C terminus of the tetrodotoxin-resistant sodium channel rNav1.9a (NaN). *J. Biol. Chem.* 276:18925–18933. <https://doi.org/10.1074/jbc.M101606200>
- Liu, C.J., S.D. Dib-Hajj, M. Renganathan, T.R. Cummins, and S.G. Waxman. 2003. Modulation of the cardiac sodium channel Nav1.5 by fibroblast growth factor homologous factor 1B. *J. Biol. Chem.* 278:1029–1036. <https://doi.org/10.1074/jbc.M207074200>
- Marban, E., T. Yamagishi, and G.F. Tomaselli. 1998. Structure and function of voltage-gated sodium channels. *J. Physiol.* 508:647–657. <https://doi.org/10.1111/j.1469-7793.1998.647bp.x>
- Matthews, E., A.Y. Manzur, R. Sud, F. Muntoni, and M.G. Hanna. 2011. Stridor as a neonatal presentation of skeletal muscle sodium channelopathy. *Arch. Neurol.* 68:127–129. <https://doi.org/10.1001/archneurol.2010.347>
- McCusker, E.C., C. Bagn eris, C.E. Naylor, A.R. Cole, N. D'Avanzo, C.G. Nichols, and B.A. Wallace. 2012. Structure of a bacterial voltage-gated sodium channel pore reveals mechanisms of opening and closing. *Nat. Commun.* 3:1102. <https://doi.org/10.1038/ncomms2077>
- Miller, T.M., M.R. Dias da Silva, H.A. Miller, H. Kwiecinski, J.R. Mendell, R. Tawil, P. McManis, R.C. Griggs, C. Angelini, S. Servidei, et al. 2004. Correlating phenotype and genotype in the periodic paralyses. *Neurology.* 63:1647–1655. <https://doi.org/10.1212/01.WNL.0000143383.91137.00>
- Napolitano, C., S.G. Priori, P.J. Schwartz, R. Bloise, E. Ronchetti, J. Nastoli, G. Bottelli, M. Cerrone, and S. Leonardi. 2005. Genetic testing in the long QT syndrome: development and validation of an efficient approach to genotyping in clinical practice. *JAMA.* 294:2975–2980. <https://doi.org/10.1001/jama.294.23.2975>
- Naundorf, B., F. Wolf, and M. Volgushev. 2006. Unique features of action potential initiation in cortical neurons. *Nature.* 440:1060–1063. <https://doi.org/10.1038/nature04610>
- Niu, J., I.E. Dick, W. Yang, M.A. Bamgboye, D.T. Yue, G. Tomaselli, T. Inoue, and M. Ben-Johny. 2018. Allosteric regulators selectively prevent Ca²⁺-feedback of Ca_v and Na_v channels. *eLife.* 7:e35222. <https://doi.org/10.7554/eLife.35222>
- Nof, E., L. Vysochek, E. Meisel, E. Burashnikov, C. Antzelevitch, J. Clatot, R. Beinart, D. Luria, M. Glikson, and S. Oz. 2019. Mutations in Nav1.5 Reveal Calcium-Calmodulin Regulation of Sodium Channel. *Front. Physiol.* 10:700. <https://doi.org/10.3389/fphys.2019.00700>
- Nu nez, E., A. Muguza-Montero, and A. Villarroel. 2020. Atomistic Insights of Calmodulin Gating of Complete Ion Channels. *Int. J. Mol. Sci.* 21:1285. <https://doi.org/10.3390/ijms21041285>
- Ou, Y., S.J. Gibbons, S.M. Miller, P.R. Strege, A. Rich, M.A. Distad, M.J. Ackerman, J.L. Rae, J.H. Szurszewski, and G. Farrugia. 2002. SCN5A is expressed in human jejunal circular smooth muscle cells. *Neurogastroenterol. Motil.* 14:477–486. <https://doi.org/10.1046/j.1365-2982.2002.00348.x>
- Pan, X., Z. Li, Q. Zhou, H. Shen, K. Wu, X. Huang, J. Chen, J. Zhang, X. Zhu, J. Lei, et al. 2018. Structure of the human voltage-gated sodium channel Nav1.4 in complex with β1. *Science.* 362:eaau2486. <https://doi.org/10.1126/science.aau2486>
- Pan, X., Z. Li, X. Huang, G. Huang, S. Gao, H. Shen, L. Liu, J. Lei, and N. Yan. 2019. Molecular basis for pore blockade of human Na⁺ channel Nav1.2 by the μ-conotoxin KIIIA. *Science.* 363:1309–1313. <https://doi.org/10.1126/science.aaw2999>
- Peters, C.H., A.R. Watkins, O.L. Poirier, and P.C. Ruben. 2020. E1784K, the most common Brugada syndrome and long-QT syndrome type 3 mutant, disrupts sodium channel inactivation through two separate mechanisms. *J. Gen. Physiol.* 152:e202012595. <https://doi.org/10.1085/jgp.202012595>
- Peterson, B.Z., C.D. DeMaria, J.P. Adelman, and D.T. Yue. 1999. Calmodulin is the Ca²⁺ sensor for Ca²⁺-dependent inactivation of L-type calcium channels. *Neuron.* 22:549–558. [https://doi.org/10.1016/S0896-6273\(00\)80709-6](https://doi.org/10.1016/S0896-6273(00)80709-6)
- Petitprez, S., A.F. Zmoos, J. Ogrodnik, E. Balse, N. Raad, S. El-Haou, M. Albesa, P. Bittihn, S. Luther, S.E. Lehnart, et al. 2011. SAP97 and dystrophin macromolecular complexes determine two pools of cardiac sodium channels Nav1.5 in cardiomyocytes. *Circ. Res.* 108:294–304. <https://doi.org/10.1161/CIRCRESAHA.110.228312>
- Potet, F., B. Chagot, M. Angheliescu, P.C. Viswanathan, S.Z. Stepanovic, S. Kupersmidt, W.J. Chazin, and J.R. Balsler. 2009. Functional Interactions between Distinct Sodium Channel Cytoplasmic Domains through the Action of Calmodulin. *J. Biol. Chem.* 284:8846–8854. <https://doi.org/10.1074/jbc.M806871200>
- Reddy Chichili, V.P., Y. Xiao, J. Seetharaman, T.R. Cummins, and J. Sivaraman. 2013. Structural basis for the modulation of the neuronal voltage-gated sodium channel Nav1.6 by calmodulin. *Sci. Rep.* 3:2435. <https://doi.org/10.1038/srep02435>
- Rivolta, I., H. Abriel, M. Tateyama, H. Liu, M. Memmi, P. Vardas, C. Napolitano, S.G. Priori, and R.S. Kass. 2001. Inherited Brugada and long QT-3 syndrome mutations of a single residue of the cardiac sodium channel confer distinct channel and clinical phenotypes. *J. Biol. Chem.* 276:30623–30630. <https://doi.org/10.1074/jbc.M104471200>
- Saimi, Y., and C. Kung. 2002. Calmodulin as an ion channel subunit. *Annu. Rev. Physiol.* 64:289–311. <https://doi.org/10.1146/annurev.physiol.64.100301.111649>
- Saito, Y.A., P.R. Strege, D.J. Tester, G.R. Locke III, N.J. Talley, C.E. Bernard, J.L. Rae, J.C. Makielski, M.J. Ackerman, and G. Farrugia. 2009. Sodium channel mutation in irritable bowel syndrome: evidence for an ion channelopathy. *Am. J. Physiol. Gastrointest. Liver Physiol.* 296:G211–G218. <https://doi.org/10.1152/ajpgi.90571.2008>
- Sarbjit-Singh, S.S., H.R. Matthews, and C.L. Huang. 2020. Ryanodine receptor modulation by caffeine challenge modifies Na⁺ current properties in intact murine skeletal muscle fibres. *Sci. Rep.* 10:2199. <https://doi.org/10.1038/s41598-020-59196-9>
- Sarhan, M.F., C.C. Tung, F. Van Petegem, and C.A. Ahern. 2012. Crystallographic basis for calcium regulation of sodium channels. *Proc. Natl. Acad. Sci. USA.* 109:3558–3563. <https://doi.org/10.1073/pnas.1114748109>
- Savio-Galimberti, E., M.H. Gollub, and D. Darbar. 2012. Voltage-gated sodium channels: biophysics, pharmacology, and related channelopathies. *Front. Pharmacol.* 3:124. <https://doi.org/10.3389/fphar.2012.00124>
- Shah, V.N., T.L. Wingo, K.L. Weiss, C.K. Williams, J.R. Balsler, and W.J. Chazin. 2006. Calcium-dependent regulation of the voltage-gated sodium channel hH1: intrinsic and extrinsic sensors use a common molecular switch. *Proc. Natl. Acad. Sci. USA.* 103:3592–3597. <https://doi.org/10.1073/pnas.0507397103>
- Shen, H., Q. Zhou, X. Pan, Z. Li, J. Wu, and N. Yan. 2017. Structure of a eukaryotic voltage-gated sodium channel at near-atomic resolution. *Science.* 355:eaal4326. <https://doi.org/10.1126/science.aal4326>
- Shen, H., D. Liu, K. Wu, J. Lei, and N. Yan. 2019. Structures of human Nav1.7 channel in complex with auxiliary subunits and animal toxins. *Science.* 363:1303–1308. <https://doi.org/10.1126/science.aaw2493>
- Shinlapawittayatorn, K., X.X. Du, H. Liu, E. Ficker, E.S. Kaufman, and I. Desch enes. 2011. A common SCN5A polymorphism modulates the biophysical defects of SCN5A mutations. *Heart Rhythm.* 8:455–462. <https://doi.org/10.1016/j.hrthm.2010.11.034>
- Singh, R.R., S.V. Tan, M.G. Hanna, S.A. Robb, A. Clarke, and H. Jungbluth. 2014. Mutations in SCN4A: a rare but treatable cause of recurrent life-threatening laryngospasm. *Pediatrics.* 134:e1447–e1450. <https://doi.org/10.1542/peds.2013-3727>
- Sochacka, M., L. Opalinski, J. Szymczyk, M.B. Zimoch, A. Czyrek, D. Krowarsch, J. Otlewski, and M. Zakrzewska. 2020. FHF1 is a bona fide fibroblast growth factor that activates cellular signaling in FGFR-dependent manner. *Cell Commun. Signal.* 18:69. <https://doi.org/10.1186/s12964-020-00573-2>
- Strege, P.R., Y. Ou, L. Sha, A. Rich, S.J. Gibbons, J.H. Szurszewski, M.G. Sarr, and G. Farrugia. 2003. Sodium current in human intestinal interstitial cells of Cajal. *Am. J. Physiol. Gastrointest. Liver Physiol.* 285:G1111–G1121. <https://doi.org/10.1152/ajpgi.00152.2003>
- Strege, P.R., A. Mazzone, C.E. Bernard, L. Neshatian, S.J. Gibbons, Y.A. Saito, D.J. Tester, M.L. Calvert, E.A. Mayer, L. Chang, et al. 2018. Irritable bowel syndrome patients have SCN5A channelopathies that lead to decreased Nav1.5 current and mechanosensitivity. *Am. J. Physiol. Gastrointest. Liver Physiol.* 314:G494–G503. <https://doi.org/10.1152/ajpgi.00016.2017>
- Tester, D.J., and M.J. Ackerman. 2005. Genetic testing for cardiac channelopathies: ten questions regarding clinical considerations for heart rhythm allied professionals. *Heart Rhythm.* 2:675–677. <https://doi.org/10.1016/j.hrthm.2004.09.024>
- Tester, D.J., M.L. Will, C.M. Haglund, and M.J. Ackerman. 2005. Compendium of cardiac channel mutations in 541 consecutive unrelated patients referred for long QT syndrome genetic testing. *Heart Rhythm.* 2:507–517. <https://doi.org/10.1016/j.hrthm.2005.01.020>
- Undrovinas, A.I., I.A. Fleidervish, and J.C. Makielski. 1992. Inward sodium current at resting potentials in single cardiac myocytes induced by the ischemic metabolite lysophosphatidylcholine. *Circ. Res.* 71:1231–1241. <https://doi.org/10.1161/01.RES.71.5.1231>
- Wang, C., B.C. Chung, H. Yan, S.Y. Lee, and G.S. Pitt. 2012. Crystal structure of the ternary complex of a Nav C-terminal domain, a fibroblast growth

- factor homologous factor, and calmodulin. *Structure*. 20:1167–1176. <https://doi.org/10.1016/j.str.2012.05.001>
- Wang, C., B.C. Chung, H. Yan, H.G. Wang, S.Y. Lee, and G.S. Pitt. 2014. Structural analyses of Ca²⁺/CaM interaction with NaV channel C-termini reveal mechanisms of calcium-dependent regulation. *Nat. Commun.* 5:4896. <https://doi.org/10.1038/ncomms5896>
- Wei, J., D.W. Wang, M. Alings, F. Fish, M. Wathen, D.M. Roden, and A.L. George Jr. 1999. Congenital long-QT syndrome caused by a novel mutation in a conserved acidic domain of the cardiac Na⁺ channel. *Circulation*. 99:3165–3171. <https://doi.org/10.1161/01.CIR.99.24.3165>
- Wisedchaisri, G., L. Tonggu, E. McCord, T.M. Gamal El-Din, L. Wang, N. Zheng, and W.A. Catterall. 2019. Resting-State Structure and Gating Mechanism of a Voltage-Gated Sodium Channel. *Cell*. 178:993–1003.e12. <https://doi.org/10.1016/j.cell.2019.06.031>
- Wu, F.F., E. Gordon, E.P. Hoffman, and S.C. Cannon. 2005. A C-terminal skeletal muscle sodium channel mutation associated with myotonia disrupts fast inactivation. *J. Physiol.* 565:371–380. <https://doi.org/10.1113/jphysiol.2005.082909>
- Yan, H., C. Wang, S.O. Marx, and G.S. Pitt. 2017. Calmodulin limits pathogenic Na⁺ channel persistent current. *J. Gen. Physiol.* 149:277–293. <https://doi.org/10.1085/jgp.201611721>
- Yoder, J.B., M. Ben-Johny, F. Farinelli, L. Srinivasan, S.R. Shoemaker, G.F. Tomaselli, S.B. Gabelli, and L.M. Amzel. 2019. Ca²⁺-dependent regulation of sodium channels Na_v1.4 and Na_v1.5 is controlled by the post-IQ motif. *Nat. Commun.* 10:1514. <https://doi.org/10.1038/s41467-019-09570-7>
- Yu, F.H., and W.A. Catterall. 2003. Overview of the voltage-gated sodium channel family. *Genome Biol.* 4:207. <https://doi.org/10.1186/gb-2003-4-3-207>
- Yu, F.H., V. Yarov-Yarovoy, G.A. Gutman, and W.A. Catterall. 2005. Overview of molecular relationships in the voltage-gated ion channel superfamily. *Pharmacol. Rev.* 57:387–395. <https://doi.org/10.1124/pr.57.4.13>
- Zaharieva, I.T., M.G. Thor, E.C. Oates, C. van Karnebeek, G. Henderson, E. Blom, N. Witting, M. Rasmussen, M.T. Gabbett, G. Ravenscroft, et al. 2016. Loss-of-function mutations in SCN4A cause severe foetal hypokinesia or ‘classical’ congenital myopathy. *Brain*. 139:674–691. <https://doi.org/10.1093/brain/awv352>